lib

EXPERIMENTAL INVESTIGATION OF SHORT-TERM PERIODICITIES IN THE QUIET-TIME X-RAY FLUX AT MID-LATITUDES

A Thesis

Presented to

the Faculty of the Department of Physics

University of Houston

In Partial Fulfillment

of the Requirements of the Degree

Master of Science

---

by

Yuan-chyau Chang

May 1971

ACKNOWLEDGEMENT

The author wishes to express his sincerest appreciation to Professor John W. Kern and Professor William R. Sheldon whose guidance, assistance and patience were invaluable throughout the work.

The author would like to thank Mr. Dennis D. Barber and Mr. Howard Leverenz for their help in reduction of the data, Dr. James R. Benbrook, Mr. Neil Sams and Mr Cary Semar for their help in computer programming.

EXPERIMENTAL INVESTIGATION OF SHORT-TERM PERIODICITIES IN THE QUIET-TIME X-RAY FLUX AT MID-LATITUDES

An Abstract of a Thesis

Presented to

the Faculty of the Department of Physics

University of Houston

In Partial Fulfillment

of the Requirements of the Degree

Master of Science

---

by

Yuan-chyau Chang

May 1971

ABSTRACT

Balloon observations of the X-ray flux of photons with energies greater than 20 keV, measured at an atmospheric depth of 8 g cm^{-2} in the vicinity of Seattle, Washington, (L = 2.7) were analyzed. The randomness of time interval t required to receive each four counts was tested using a modified duration-distribution law. The technique of power spectral analysis was used to investigate periodicities in the flux. Statistically significant peaks were found in the spectral power density of this high altitude X-ray data, although neither pulsation nor microburst phenomena were present. Count rates based on different time intervals were used to investigate the periodic nature of the flux. The peaks were found in the X-ray power spectra at periods corresponding to the bounce periods of electrons in the energy range 20 to 400 keV. This observation indicates that the observed X-ray fluxes at L = 2.7 were influenced by trapped electrons in the magnetosphere on this L shell.

TABLE OF CONTENTS

1. INTRODUCTION

Since the discovery of electron precipitation in the auroral zone (Van Allen 1955), considerable interest has developed in various aspects of the aurora. Numerous balloon, rocket and satellite studies have investigated this kind of radiation and its association with other geophysical phenomena. The understanding of electron precipitation has been increased by these experiments. Direct measurements by detectors on rockets and satellites provide accurate estimates of the flux and energy spectrum of auroral electrons. Indirect measurements of auroral electrons have been made by observing the resulting auroral X-rays from high-altitude balloons. Through these investigations it has been possible to make observations for longer periods of time at relatively fixed positions; these investigations have contributed greatly to the progress in this area of research.

Radiation in the atmosphere and the trapped radiation just above is influenced by the geomagnetic field. The magnetic field of the earth is fairly complicated, however the dipole component is much larger than higher order components. The L parameter was introduced by McIlwain (1961) to describe the behavior of charged particles in the geomagnetic field, taking into account the complex nature of the field, yet taking advantage of the largely dipole nature of the field. L is constant along a line of force and labels the magnetic shell on which an electron is trapped, bouncing in latitude and drifting in longitude. Numerically, L is equal to the average equatorial radius of the magnetic shell, measured in units of earth radii. The relatively small range of latitude in the auroral zone corresponds to a very large region on the equatorial plane as shown in Fig. 1.

The precipitation of energetic electrons in the auroral zone is frequently detected through the measurement of X-rays at balloon altitudes. Electrons precipitate into the upper atmosphere and produce the bremsstrahlung photons with energies comparable to the kinetic energies of the electrons. Some of the photons diffuse down to balloon altitudes and are detected.

The large fluctuations in intensity has been recognized as one of the remarkable features of the auroral-zone X-ray fluxes (Anderson, 1964). Both the spatial and temporal variations of these X-rays have been studied during the past ten years. Observations of X-ray fluxes at an altitude greater than thirty km provides a means of investigating the development of electron precipitation events and their connection with disturbances of the geomagnetic field.

It is well known that electron precipitation events occur more often in the range of $5 < L < 8$ than for either larger or smaller L values. The most notable precipitation events give rise to displays of visual aurora which are frequently observed in this region and lead to it being called the auroral zone. The spatial correlation of X-ray fluxes for different latitudes and longitudes has been investigated by several groups (Brown et al., 1963, 1965; Parks et al., 1965; Parks, 1967). The fluxes were found to be quite different, both with or without magnetic disturbance, even by simultaneous balloon observations. No strong correlation between data collected in balloons apart either in the north-south or in the east-west directions could be found. The significant dissimilarity of X-ray fluxes observed by balloons with spatial separations of approximately 200 to 300 km led to the conclusion that the electron precipitation is highly localized even within the auroral-zone region.

In addition, a variety of simultaneous geomagnetically conjugate-area balloon experiments have been conducted in the northern and southern hemispheres (Anderson et al., 1962; Brown et al., 1963; Brown et al., 1964, 1965). Although similar activity has been reported at auroral latitudes in each hemisphere, no good correlation between conjugate points has been found. This may be due to the difficulty in establishing conjugate points in each hemisphere. In simultaneous electron precipitation measurements (Brown et al., 1965) in the northern and southern auroral zones, the counting rates are quite different for identical detectors and the time profiles bear little resemblance to one another. This may be due to the fact that the separation of the ballons in latitude and longitude was appreciable at all times during the flight. According to the interpretation of Anderson (1964), the results show that the electron precipitation occurs from distinctly separate bundles of magnetic lines. It was only for a short time period that detectors in the northern and southern auroral zones registered a very large flux of X-rays simultaneously. In this particular event the precipitation became very widespread and both balloons were within the same general precipitation pattern. For such events, Anderson infers that a very large region of the magnetosphere is involved in the precipitation progress. The size of this region must be on the order of 1000 km in width and 3000 km in depth if it lies near the equatorial plane.

Fast time variations in electron precipitation have been investigated by several groups. During the balloon flights, Anderson and Milton (1964) identified a new type of auroral X-ray event using large area detectors and fast response circuitry. The precipitation events (called microbursts) were found to occur singly at times, but more often in groups of two or more. The highly variable microburst events were superimposed on a smooth quiet-time X-ray background. The time profiles of microbursts have been a subject of discussion in the literature. Anderson and Milton (1964) found the microbursts to be symmetrical in time and about 0.25 seconds in duration at the point of half maximum. Venkatesan et al. (1968) reported microbursts have a harder characteristic energy spectrum, a faster rise time (the order of 30 msec) and a decay time of the order of 200 msec. The spatial extent of precipitation microbursts was rather limited in comparison with other forms of auroral zone electron precipitation which extend thousands of km in longitude and several hundred km in latitude during magnetic storm conditions. Parks (1967) estimated the spatial extent for each microburst precipitation region to be on the average 40±14 km radius on the X-ray production plane; for some microbursts, the precipitation regions are smaller than 20 km in radius.

X-ray precipitation events have been observed both with and without accompanying local magnetic disturbances, indicating that electron precipitation is possible under a variety of circumstances; however, these events have been detected more frequently during disturbed periods than during the periods of relatively quiet geomagnetic conditions (Anderson, 1964). Associated with the occurrence of a strong magnetic bay, auroral activity has been detected deep within the magnetospace, down to $L \approx 3$. The large number of X-ray measurements in the auroral zone suggest that at least some of these events at lower latitudes have accompanying X-ray activity. However, there have been only a small number of investigations of atmospheric X-rays at middle and lower latitudes and auroral activity in these regions occurs infrequently.

Investigations of time variations in the X-ray flux have helped to determine the behavior of electron precipitation. Balloon observations of bremsstrahlung X-ray fluxes have revealed a variety of characteristic periodicities in the precipitated electron flux. Herein is reported an experimental study of time variations in the quiet time X-ray flux with high resolution which was made in the middle latitude region about halfway between the equatorial region and the auroral zone. An investigation of X-ray precipitation features at mid-latitudes will aid in the construction of the theoretical models of the magnetosphere and lead to greater understanding of magnetosphere phenomena. It is the purpose of this analysis to systematically study the temporal structure of the bremsstrahlung X-rays, in order to gain a better understanding of electron precipitation.

2. OBSERVATIONS

A measurement of X-ray intensity at an atmospheric depth of 8 gm/cm^2 was made on June 25, 1964 from a balloon in the vicinity of Seattle, Washington (L = 2.7). The X-ray flux was measured with an unshielded NaI scintillation crystal. The output pulses of the photomultiplier were applied to the inputs of four integral discriminators with energy levels of greater than 20 keV, 50keV, 100 keV and 200 keV. Each discriminator output was divided by eight in a scaler so that each transition of the scaler corresponds to four counts. The scaler outputs drive four subcarrier oscillators of frequencies 5.4 kHz for $E > 20$ keV, 3.9 kHz for $E > 50$ keV, 3.0 kHz for $E > 100$ keV and 2.3 kHz for $E > 200$ keV. The outputs of the subcarrier oscillators were mixed, amplified and used to modulate a 227 MHz transmitter. A diagram of the flight apparatus is shown in Figure 2. The data (mixed subcarrier signals) from the output of a telemetry receiver was recorded on 1/4 inch magnetic tape at 7.5 inches per second. Subcarrier discriminators were used to separate the channels during playback of the magnetic tape and data processing apparatus printed out the time duration for each four counts above a particular energy level.

The energy spectrum and the counting rate curves during the ascent to altitude are shown in Figure 3. The differential X-ray energy spectrum was compared with those of other workers as shown in Figure 4.

A fifteen minute segment of continuous data at ceiling altitude (105,000 ft) was selected for detailed temporal analysis. The first step in the analysis of the time variation is a simple visual examination of the curves of counting rate versus time. The data was artificially divided into ten consecutive sections, each section containing 90 seconds. These data, averaged over intervals of 1.0 second, are shown in Figure 5; the average counting rate, C, of each section is also shown. The rate of change of the average counting rate during the ten sections is small. By visual examination, fluctuations of the counting rate do not appear to be greater than would be expected for a random source. In only one portion of the third section is the counting rate appreciably lower than average. Neither pulsations nor microbursts were found in a visual examination of the data.

3. ANALYTICAL METHODS

In the experimental data analysis, a number of analytical methods were used to examine the time-dependence of the observed X-ray flux and to test the possibility of the flux exhibiting distribution patterns which indicate coherent modulation of the X-ray source.

(1). Frequency - Duration Distribution

All random processes whose probability of occurrence is small and constant are described by the Poisson distribution. If $\overline{X}$ is the average constant value, then the probability P_X that X will occur is

$$P_X = \frac{\overline{X}^X}{X!} e^{-\overline{X}} \tag{1}$$

Let c be the average rate of appearance of particles; then the average number of events in a time interval t is ct. The probability $P_X(t)$ of observing X particles during time t is

$$P_X(t) = \frac{(ct)^X}{X!} e^{-ct} \tag{2}$$

When a scaling circuit is used, one output pulse is produced for every n input events. In this case we proceed by calculating the combined probability of (n-1) events occuring in time t and one additional event (the nth) occuring between t and t + dt as follows,

$$dp_t = \left(\frac{(ct)^{n-1}}{(n-1)!} e^{-ct}\right)(c\,dt)$$

$$= \frac{c^n t^{n-1}}{(n-1)!} e^{-ct}\,dt \qquad (3)$$

Equation (3) expresses the probability that an n-fold interval will have a duration between t and t + dt. So, the probability that an n-fold interval will have a duration between T_1 and T_2 is

$$\int_{T_1}^{T_2} dp_t = \frac{c^n}{(n-1)!}\int_{T_1}^{T_2} t^{n-1} e^{-ct}\,dt$$

$$= \frac{c^n}{(n-1)!}\left\{\int_0^{T_2} t^{n-1} e^{-ct}\,dt - \int_0^{T_1} t^{n-1} e^{-ct}\,dt\right\}$$

The integral $\int_0^T t^{n-1} e^{-ct}\,dt$ can be evaluated by successive integration by parts, yielding

$$\int_0^T t^{n-1} e^{-ct}\,dt = \frac{(n-1)!}{a^n}\left\{1 - e^{-cT} - \frac{cT}{1} e^{-cT} - \frac{(cT)^2}{2!} e^{-cT} \cdots\cdots - \frac{(cT)^{n-1}}{(n-1)!} e^{-cT}\right\}$$

So, the probability becomes

$$\int_{T_1}^{T_2} dp_t = \left\{1 - e^{-cT_2} - \frac{T_2}{1} e^{-cT_2} - \frac{cT_2}{2!} e^{-cT_2} \cdots\cdots\cdots - \frac{(cT_2)^{n-1}}{(n-1)!} e^{-cT_2}\right\}$$

$$-\left\{1 - e^{-cT_1} - \frac{T_1}{1} e^{-cT_1} - \frac{cT_1}{2!} e^{-cT_1} \cdots\cdots\cdots - \frac{(cT_1)^{n-1}}{(n-1)!} e^{-cT_1}\right\}$$

$$-\left\{e^{-CT_1}-e^{-CT_2}\right\}+\left\{T_1e^{-CT_1}-T_2e^{-CT_2}\right\}+\left\{\frac{(CT_1)^2}{2!}e^{-CT_1}-\frac{(CT_2)^2}{2!}e^{-CT_2}\right\}$$

$$+\cdots\cdots+\left\{\frac{(CT_1)^{n-1}}{(n-1)!}e^{-CT_1}-\frac{(CT_2)^{n-1}}{(n-1)!}e^{-CT_2}\right\} \qquad (4)$$

A Chi-square test was used to examine the fit of the observed data to the above theoretical distribution. This test provides a statistical determination of the probability that the experimental data was the result of random processes. Chi-square is defined:

$$\chi^2=\sum_i \frac{\left\{(\text{observed Value})_i-(\text{expected Value})_i\right\}^2}{\left\{\text{expected Value}\right\}_i} \qquad (5)$$

This quantity and the number of degrees of freedom (which constitute the number of independent classifications in which the observed series of data may differ from the hypothetical value) together with a suitable interpretation constitute the Chi-square test.

(2). Power Spectrum Analysis

To make a more systematic study of possible modulation of the X-ray data, the technique of the power spectrum (Blackman et al., 1958) was used. This has been recognized as one of the most useful tools in handling large amounts of data, especially when conducting a search for so-called hidden periodicities. The procedure used for the present work was based on the method of Parzen (1964) who developed a method of empirical time series analysis which could be used with standard data handling procedures.

The starting point in spectral analysis is a time series $\{X(t), t = 1, 2, \cdots\cdots\}$ which is written as the sum of its average value and fluctuations from the average.

$$X(t) = \overline{X}(t) + Y(t) \tag{6}$$

If the quantities in the series have a time dependent relation, then, in addition to the average and the variance, the covariance between the values of X(t) are correlated. In order to perform a statistical analysis of X(t) to determine the presence of a time-dependent relationship between the quantities, we proceed by assuming X(t) is stationary, i.e. that time-dependent properties are a function of the difference $(t_i - t_j)$ rather than depending on t_i, or t_j

$$\begin{aligned} COV(v) &= AVE\{(X(t) - \overline{X})\ (X(t+v) - \overline{X})\} \\ &= AVE\{Y(t)\ Y(t+v)\} \end{aligned} \tag{7}$$

Thus, a stationary time series analysis assumes that the average $\overline{X}$, the variance σ^2 and the covariance COV(v) provide a complete description of X(t). However the spectral density function f(w), the Fourier transform of COV(v), is more often used instead of the covariance. To illustrate the properties of the spectral density function, Jenkins (1964) assumed that X(t) was a superimposed alternating voltage of average $\overline{X}$, various frequencies W_i, amplitudes A_i and phases ϕ_i relative to an arbitrary origin.

$$X(t) = \overline{X} + \sum_i A_i \cos(W_i t + \phi_i) \qquad (8)$$

If X(t) is measured in volts, the instantaneous power generated in a given resistance at time t is proportional to $X^2(t)$ measured in watts. The average power per complete cycle is

$$AVE = \{X^2(t)\} = \bar{X}^2 + \tfrac{1}{2}\sum_i A_i^2 \qquad (9)$$

The time dependent part may be written as

$$AVE = \{X(t) - \bar{X}\}^2 = \tfrac{1}{2}\sum_i A_i^2 \qquad (10)$$

The above equation is simply the variance (of the function X(t)) which may be regarded as being composed of components (of power) corresponding to each frequency.

If X(t) is a more general statistical fluctuation, in addition to the components of power variance due to the periodic terms, there is a further term representing contributions to the total variance from a continuous spectrum of frequency w,

$$\sigma^2 = \int_0^\infty F(w)\,dw + \frac{1}{2}\sum_i A_i^2 \qquad (11)$$

Combining these two terms

$$\sigma = \int_0^\infty F'(w)\,dw$$

In normalized form, this becomes

$$1 = \int_0^{\infty} \frac{F'(w)}{\sigma^2}\, dw$$

or

$$1 = \int_0 f(w)\, dw \qquad (12)$$

where $f(w) = \frac{F'(w)}{\sigma^2}$ is called the spectral density function.

The usefulness of a Fourier series is that it enables one to represent a function F(t) approximately as a harmonic polynomial of some finite degree n.

$$F(t) \approx F_n(t) = \sum_n \left\{ A_n \cos W_n t + B_n \sin W_n t \right\} \qquad (13)$$

where

$$A_0 = \frac{1}{T}\int_0^T f(x)\, dx \;,$$
$$B_0 = 0,$$
$$A_n = \frac{2}{T}\int_0^T f(x) \cos W_n x\, dx, \quad \text{and}$$
$$B_n = \frac{2}{T}\int_0^T f(x) \sin W_n x\, dx \;.$$

$F_n(t)$ can be represented in terms of F(t), for $n \geq 1$

$$A_n \cos W_n t + B_n \sin W_n t$$
$$= \frac{2}{T}\int_0^T f(x) \left\{ \cos W_n t \cos W_n x + \sin W_n t \sin W_n x \right\} dx$$
$$= \frac{2}{T}\int_0^T f(x) \cos W_n (x - t)\, dt$$

Consequently,

$$F_n(t) = \frac{1}{T}\int_0^T (1 + 2\cos w_1(x-t) + \cdots + 2\cos w_n(x-t)) f(x)\,dx$$

$$= \int_0^T \frac{1}{T} D_n\left(2\pi \frac{x-t}{T}\right) f(x)\,dx \qquad (14)$$

where

$$D_n(t') = 1 + \cos t' + 2\cos 2t' + \cdots\cdots + 2\cos nt'$$

$$= \frac{\sin(n+\frac{1}{2})t'}{\sin\frac{1}{2}t'} \qquad (15)$$

The function $D_n(t')$ is called Dirichlet's kernel. Equation (14) shows that the harmonic polynomial $F_n(t)$ is actually an integral averaging over the values of F(t) weighted by the kernel $\frac{1}{T}D_n\left(2\pi\frac{x-t}{T}\right)$. As can be shown, Dirichlet's kernel is not a satisfactory "window" for numerical analysis (Blackman et al., 1958). Various kernels have been developed for better estimates of a Fourier transform.

As an estimate of the spectral density function f(w), we can take (Parzen, 1964)

$$f(w) = \frac{1}{2\pi} \sum_{v \le M} e^{ivw}\, k\left(\frac{v}{M}\right) COV(v) \qquad (16)$$

which depends on a choice of three quantities:

(A). An integer M, called the truncation point of the spectral estimate.

(B). A kernel k(·) knwon as the lag window of the spectral estimate

(C) The number of points on the interval between 0 and π which are to be computed

$$w = 0, \frac{\pi}{\theta}, \frac{2\pi}{\theta}, \cdots\cdots\cdots \frac{\theta}{\theta}\pi$$

4. RANDOM TEST

The original data consisted of measurements of the time duration Δt required to receive each four counts. In order to test the randomness of the data statistically, first the distribution function of probability for Δt was calculated. A computer program was written to compute the theoretical value of the distribution function in Δt (equation 4) using a scale factor of four and the calculated curve was compared with the experimental results.

The theoretical curves depend on the average counting rate. For a lower average counting rate, the curve shifts to the right and the peak is lower. For a higher average counting rate, the curve shifts to the left and the peak is higher. Both the theoretical curve and the experimental results for one section of the data are shown in Figure 6 where it can be noted that the experimental values fluctuate around the theoretical curve. The magnitude of the fluctuations are not unreasonable. For the peak value of 144 events, the probable error is $0.67 \times \sqrt{144} = 8$ events. This means that for a completely random process the deviation of an experimental value from the theoretically calculated value has an equal probability (50%) to be greater or smaller than 8 events. The remaining sections show similar tendencies, except that the third section contains a portion with a low counting rate as mentioned previously.

The Chi-square for each section was also computed to test the fit of the data to a random process. The results are shown in Table 1. From the Chi-square table for twelve degrees of freedom, the Chi-square value has an equal probability to be greater or smaller than 11.34. In Table 1, it can be seen that four of the ten sections of data had values of Chi-square less than 11.34 and six sections had larger values, in good agreement with *a priori* statistical expectations.

5. PERIODICITIES

A more systematic study of periodicities in the X-ray data was made by examining the frequency content of the flux. First the entire fifteen minutes of data, averaged in 1-second intervals, were analyzed using the power spectrum programs. The procedure of computation is to form the autocorrelation of the counting-rate variation at a given lag value v, given by the relation:

$$COR(v) = COV(v) \Big/ (S_0, S_v)^{\frac{1}{2}}$$

where COV(v), the autocovariance, is given by

$$COV(v) = \frac{1}{N-v} \sum_{t=1}^{N-v} (x_t - \bar{x}_0)(x_{t+v} - \bar{x}_v)$$

with

$$\bar{x}_0 = \frac{1}{N-v} \sum_{t=1}^{N-v} x_t$$

$$\bar{x}_v = \frac{1}{N-v} \sum_{t=v+1}^{N} x_t$$

$$S_0 = \frac{1}{N-v} \sum_{t=1}^{N-v} (x_t - \bar{x}_0)^2$$

$$S_v = \frac{1}{N-v} \sum_{t=1}^{N-v} (x_{t+v} - \bar{x}_v)^2$$

The autospectral density function is then computed. For the lag v, v = 0, 1, 2, -----, M the normalized autospectral density function at period P, P = 0, 1, 2, -----, Q is given by

$$f(p) = \frac{1}{2\pi}\left\{ COR(0) + \sum_{V=1}^{M} k\left(\frac{V}{M}\right) \cos\left(\frac{2\pi V}{P}\right)\left(COR(V)+COR(V)\right)\right\}$$

The normalized autospectral density function at frequency f, $f = \frac{1}{Q}, \frac{2}{Q}, \frac{3}{Q}, \cdots\cdots \frac{Q}{Q}$, is given by

$$f(f) = \frac{1}{2\pi}\left\{ COR(0) + \sum_{V=1}^{M} k\left(\frac{V}{M}\right) \cos\left(\frac{2\pi V \times 100 f}{Q}\right)\left(COR(V)+COR(V)\right)\right\}$$

where the spectral window k(·) is defined (Parzen 1964) as

$$\begin{aligned} k(u) &= 1 - 6u^2 + u^3 , & 0 \leq u \leq 0.5 \\ &= 2(1-u)^3 , & 0.5 \leq u \leq 1 \\ &= 0 , & u \geq 1 \end{aligned}$$

Figure 7 shows the power spectrum of 900 data points with the number of lags M = 36. The high peak at lowest frequency was apparently due to the influence of the low counting rate portion in section 3. No appreciable peak appears for any frequency.

The tendency of increasing amplitude for higher frequency suggests the possibility of having shorter periodicities in the data. Thus, the measurements were again analyzed using averages over 0.1-second intervals. Power spectra were computed for ten consecutive sections and the results are shown in Figure 8.

The variance of the estimated spectral density depends on the truncation point M, sample size N, the kernel k(·) and the true spectral density function f(w). To avoid large variance or bias of an estimate of f(w), appropriate choice of M is important. In our X-ray data analysis, several choices of truncation point were made to give a better picture of the spectra and to avoid false peaks. The effective frequency which could be examined ranges from 0.05 second^{-1} to 0.5 second^{-1}. The range of periods which can be investigated with the power spectrum depends on the time interval Δt used for averaging data. This technique gives best spectral estimate at two to twenty times the time interval.

The bounce period for an electron, the time required for an electron to travel from one mirror point to its conjugate point and back, depends on the electron energy and the L value of the geomagnetic field as shown in Figure 9. The bounce periods for electrons with energies from 20 keV to 400 keV at L = 2.7 range from 0.25 sec to 1.2 sec. The power spectrum for 0.1-sec interval gives the best spectral estimate for periods of 0.2 sec to 2.0 sec. So, the 0.1-sec interval is the best time interval for establishing power spectral densities with periods of the order of an electron bounce period (for electron energies of 20 keV to 400 keV).

From an examination of Figure 8, it is apparent that most of the sections of data have statistically significant peaks. But the variability of the frequencies of the peak for each section indicates the nonstationary character of any periodicities which would be associated with the precipitation of trapped electrons.

The data were also analyzed for a time interval of 0.05-sec which gives an effective spectral estimate from a period of 0.1 sec to 1 sec. Power spectra were computed for each two adjoining sections of data and are shown in Figure 10. From a comparison of Figure 10 with Figure 8, the remarkable observation is that the amplitude apparently decreased with the increase of frequency in Figure 10, whereas in Figure 8 this is not the case. This observation can be explained in terms of electron bounce periods and the fact that the characteristic times involved cover the full range of frequencies examined in Figure 8; however electrons in the energy range 20 to 400 keV, having bounce periods of 1.2 to 0.25 sec can contribute only to the lefthand portion of the power spectra shown in Figure 10. It can be seen that the portions of Figure 10 are enhanced in the range of frequencies corresponding to trapped electron bounce periods.

The comparison of Figures 8 and 10, taken with the statistically significant peaks seen in both figures is interpreted as evidence that trapped electrons are contributing a measurable fraction of the X-ray flux measured in the mid-latitude region at high altitudes. Further investigation, using large area detectors to eliminate any statistical uncertainty, appears to be indicated by this study.

6. DISCUSSION

Electron precipitation in the auroral zone is a frequently-occurring phenomenon with an average daily rate of the order of 10^{10} and 10^{11} electrons/cm^2 (Anderson, 1960; Brown, 1960). Estimates of electron fluxes based on X-ray observations at balloon altitudes vary over a wide range, from negligible amounts during quiescent conditions to 10^9 electrons/cm^2-sec during geomagnetically disturbed periods. Several kinds of variations are superimposed on the smooth X-ray background, ranging from long-period pulsations to short-term microburst phenomena. Small amounts of precipitation electrons can be supplied from particles trapped in the geomagnetic field (i.e. from the radiation belts). But for the high intensity fluxes observed during strong geomagnetic disturbances, the insufficiency of the trapped radiation can be seen by comparing the particle loss to the available supply of trapped particles. The number of electrons in a magnetic tube whose ends have areas of 1 cm^2 at the auroral zone is about 10^{10} electrons/cm^2 (O'Brien, 1964), so an average flux of the order of 10^6 electrons/cm^2-sec could be maintained for only 10^3 to 10^4 seconds without exhausting the supply of trapped electrons; the intense electron precipitation observed in auroral events would exhaust the available supply in a few seconds. Thus, additional acceleration or supply mechanisms must be involved, at least during intense geomagnetic disturbances.

For the long-period pulsations, a model of modulation involving a traveling hydromagnetic disturbance has been suggested (Barcus and Christensen, 1965). A local acceleration is assumed to exist over a large equatorial portion of the magnetosphere at around L = 6. The hydromagnetic waves present in the magnetosphere in the acceleration region produce a means of modulating electron precipitation. Under ambient field conditions, only electrons produced with pitch angles smaller than θ are able to reach the auroral atmosphere. Where θ is given by

$$\frac{\mathrm{Sin}^2\theta}{B} = \frac{1}{Bm},$$

Bm being the mirror point field strength. The precipitation cone is of the size of

$$\begin{aligned}\Omega &= 2\pi(1 - \mathrm{Cos}\theta)\\ &\approx \pi\ \mathrm{Sin}^2\theta\\ &\approx \pi\ \frac{B}{Bm}\end{aligned}$$

When the region is perturbed by a longitudinal hydromagnetic disturbance, the effective size of the precipitation cone changes

$$\frac{\Delta\Omega}{\Omega} \approx \frac{\Delta B}{B}$$

The intensity of precipitation is therefore modulated with a relative amplitude $\frac{\Delta I}{I} = \frac{\Delta B}{B}$ and at the wave frequency.

The features of short-duration microbursts have been studied by several groups for further understanding of the processes involved in this type of electron precipitation. For different regions of origin, different precipitation processes are indicated. Based on the fact that the power spectrum of the auroral zone X-ray data shows a (barely significant) peak at 0.6 sec period, a time which is half the bounce period for 100 keV electrons at L = 6, Anderson and Milton (1964) suggested that microbursts arise from disturbances which originated in the outer magnetosphere and propagate inward, releasing electrons trapped on the L = 6 line of force. The temporal features of the microburst phenomena were explained in terms of the dynamics of energetic electrons. Magnetic pulsations, with amplitudes from a few gammas to 100 gammas, are found in the outer magnetosphere (Sonnet et al., 1963). These sharp pulses produce disturbances on the L = 6 line of force where microbursts are detected. The equatorial portion of the L = 6 field line is exposed to these disturbances. Electrons of 100 keV energy in this region having appropriate pitch angles require 0.2 seconds to precipitate into the atmosphere. This electron travel time could explain the characteristic width of the microbursts. Particles in the loss cone giving rise to an observed microburst enter the atmosphere and are lost. Particles just outside the loss cone move back to the equatorial disturbed region and scatter into the loss cone. These particles then precipitate into the atmosphere about 0.6 sec after the initial burst. The process would continue until the disturbance is not able to scatter electrons into the loss cone.

This model successfully explains the characteristic times of microbursts. But an exceptionally high velocity of propagation is required for the disturbance to sweep across the acceleration region so fast that the width of a microburst is determined solely by electron dynamics. The fact that microbursts are highly localized in space is not easy to explain in terms of the propagation model. To deal with these difficulties, Brown and Barcus (1965) suggested that microbursts arise during disturbed conditions as a result of local instabilities in the magnetospheric plasma rather than as a result of a propagating disturbance. On this basis, the characteristic times are related to the buildup and release of plasma instabilities.

Other workers have reported a variety of periodicities in auroral zone X-ray fluxes over a wide range of values, from a few tenths of a second to 100 seconds or more. The objective of investigating these periodicities is to provide a basis for discovering the mechanisms which cause electron precipitation. Because of the broad spectrum of values for periodicities and the complication of the temporal structures, a single acceleration mechanism is not able to explain all of the observed temporal behavior. However the observed periodicities have often been in the range of frequencies corresponding to bounce periods of trapped electrons, and this observation has consequently led to models involving the dynamics of these particles.

There are no studies with which the present study can be directly compared. Only a few measurements have been made of the quiet-time flux of atmospheric X-rays at locations other than in the auroral zone, and the other studies do not present the fast-time resolution which has been a significant feature of the present study. The notable result of the present study is that statistically significant peaks were found in the high altitude X-ray data with periods corresponding to the bounce periods of electrons in the energy range 20 to 400 keV. These peaks were discovered by the technique of power spectrum analysis and the enhancement of spectral power at these frequencies can be seen in two ways. They appear as non-stationary (in time) concentrations of power at various frequencies when the frequency range under investigation coincides with the frequency range of mirroring electrons. When only a portion of the frequency range under investigation is related to electron bounce periods, the power is found to be systematically depressed at higher frequencies. These effects were noted in Figure 8 and through a comparison of Figures 8 and 10.

The conclusion of this study is that the observed X-ray fluxes at L = 2.7 were influenced by trapped electrons in the magnetosphere on this L shell. The simplest explanation is that precipitation of trapped electrons was observed. This explanation is consistent with the sudden depletions of trapped electrons observed with satellite instruments (O'Brien, 1962, 1964; Paulikas et al., 1964; Paulikas et al., 1966). However, an explanation of the present results in terms of local instabilities in the magnetospheric plasma cannot be excluded. It is interesting to note that periodicities at electron bounce periods are a significant feature of the present result in the mid-latitude region and of a number of results from auroral zone studies. The auroral work cannot be used for a direct comparison because it differs in two important aspects. The contribution to the counting rates at frequencies of interest in the present result is only a small fraction of the quiet-time background rate, whereas in the auroral studies it was often observed to be many times greater. Also, the electron energy spectrum in auroral precipitation events has been determined (Anderson et al., 1960; Bhavsar, 1961) to be typically quite steep, decreasing in intensity sharply with increasing energy; the energy spectrum of trapped electrons at L = 2.7 is significantly less steep, with an e-folding energy several times that of auroral electrons. Despite these differences between electrons in auroral zone precipitation events and trapped electrons at $L = 2.7$, it is conceivable that local instabilities in the magnetospheric plasma could provide an explanation for the modulation in both regions. Additional measurements should be made using a much larger detector which would reveal more significant features of the modulation of the flux of atmospheric X-rays.

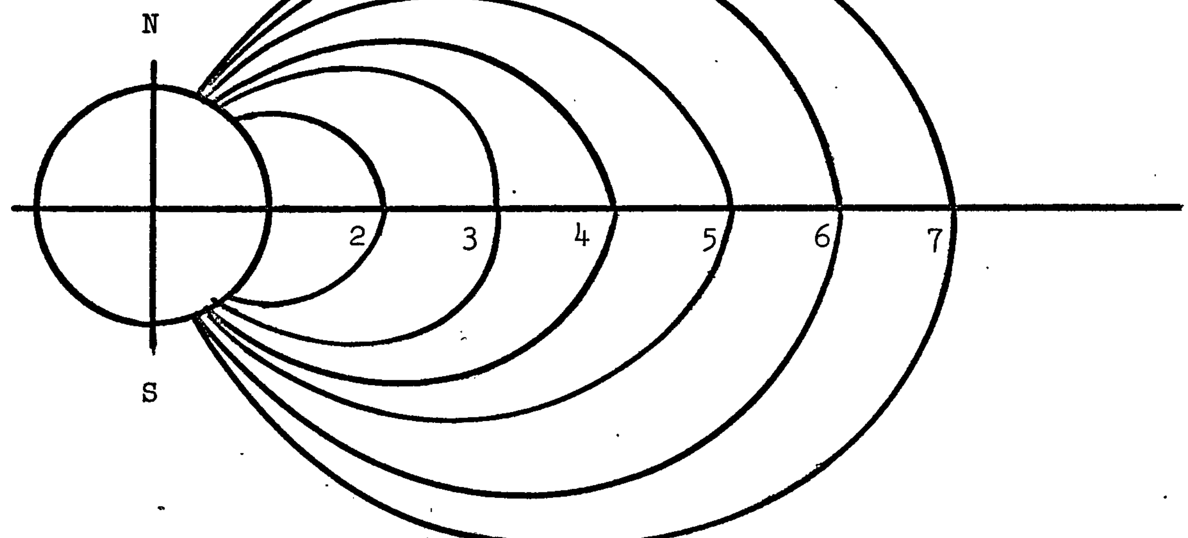

Fig. 1

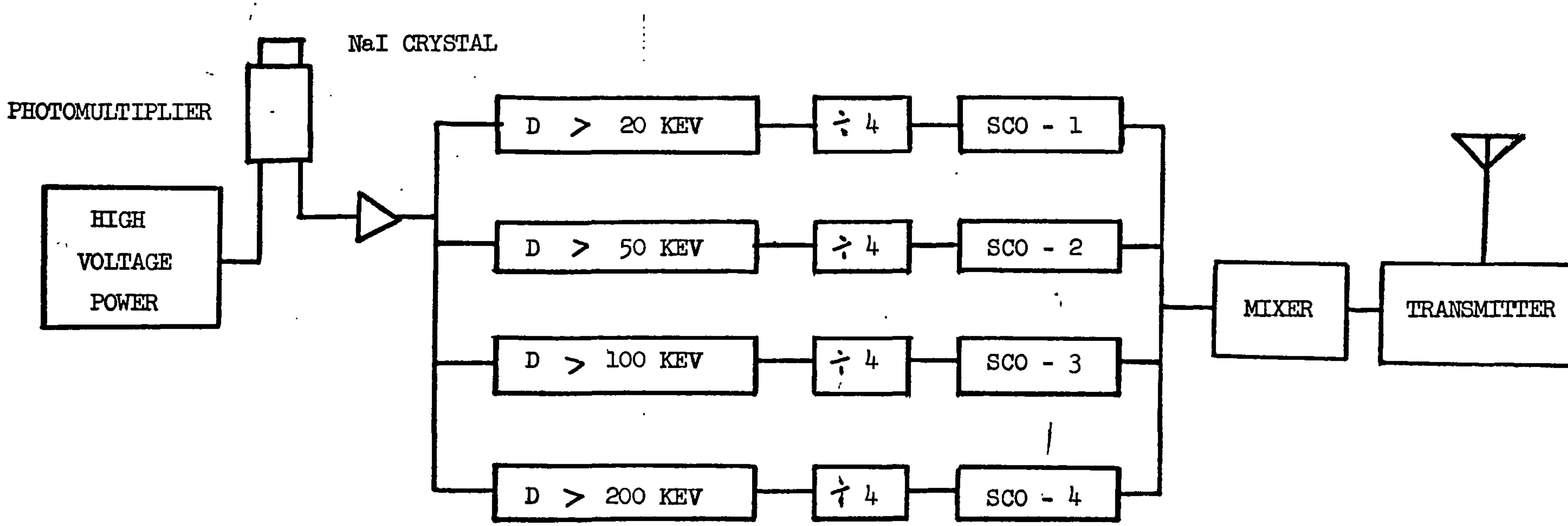
NaI CRYSTAL
PHOTOMULTIPLIER
HIGH VOLTAGE POWER
D > 20 KEV
D > 50 KEV
D > 100 KEV
D > 200 KEV
÷ 4
÷ 4
÷ 4
÷ 4
SCO - 1
SCO - 2
SCO - 3
SCO - 4
MIXER
TRANSMITTER

Fig. 2

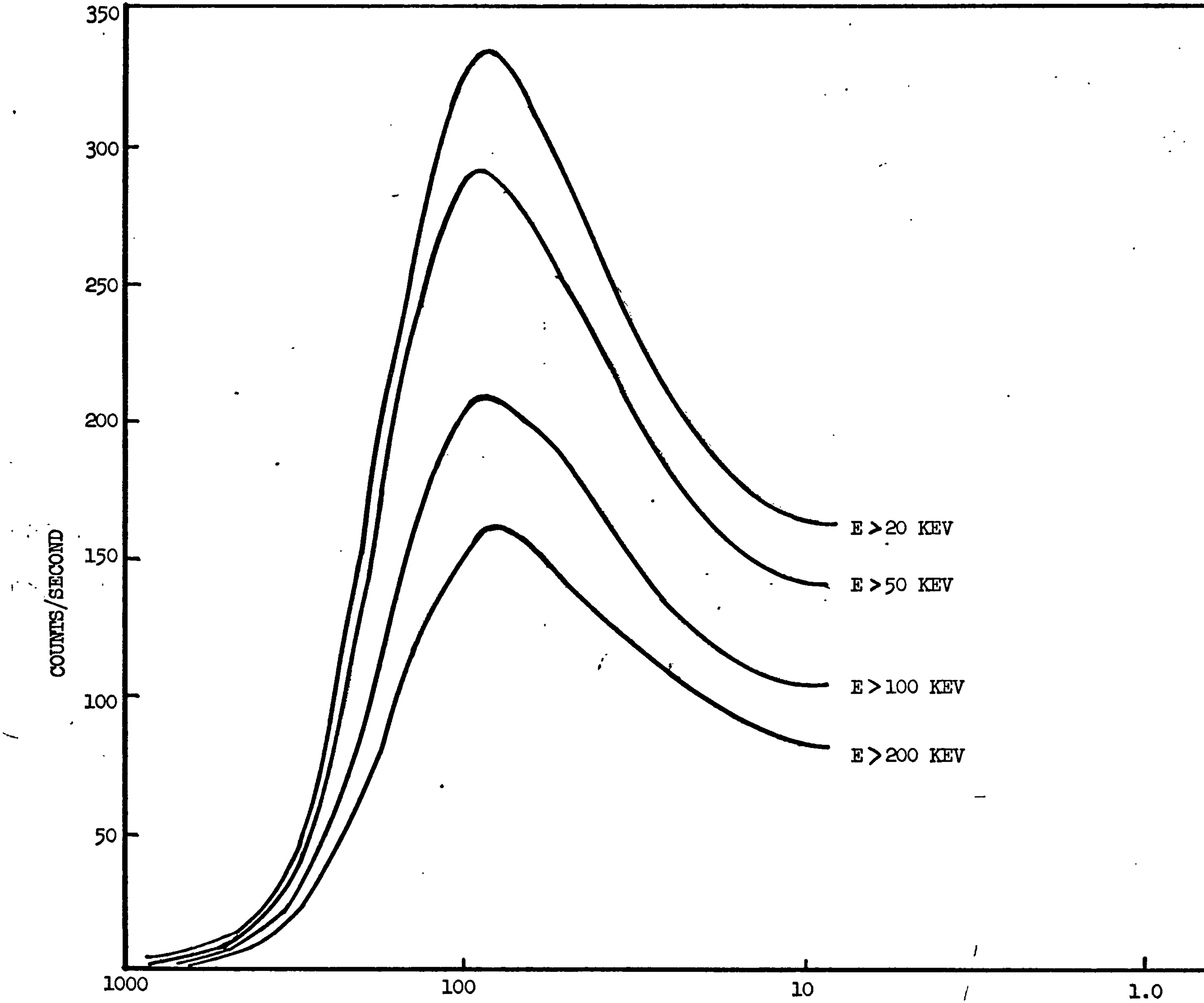

Fig. 3 ATMOSPHERIC DEPTH (gm/cm^2)

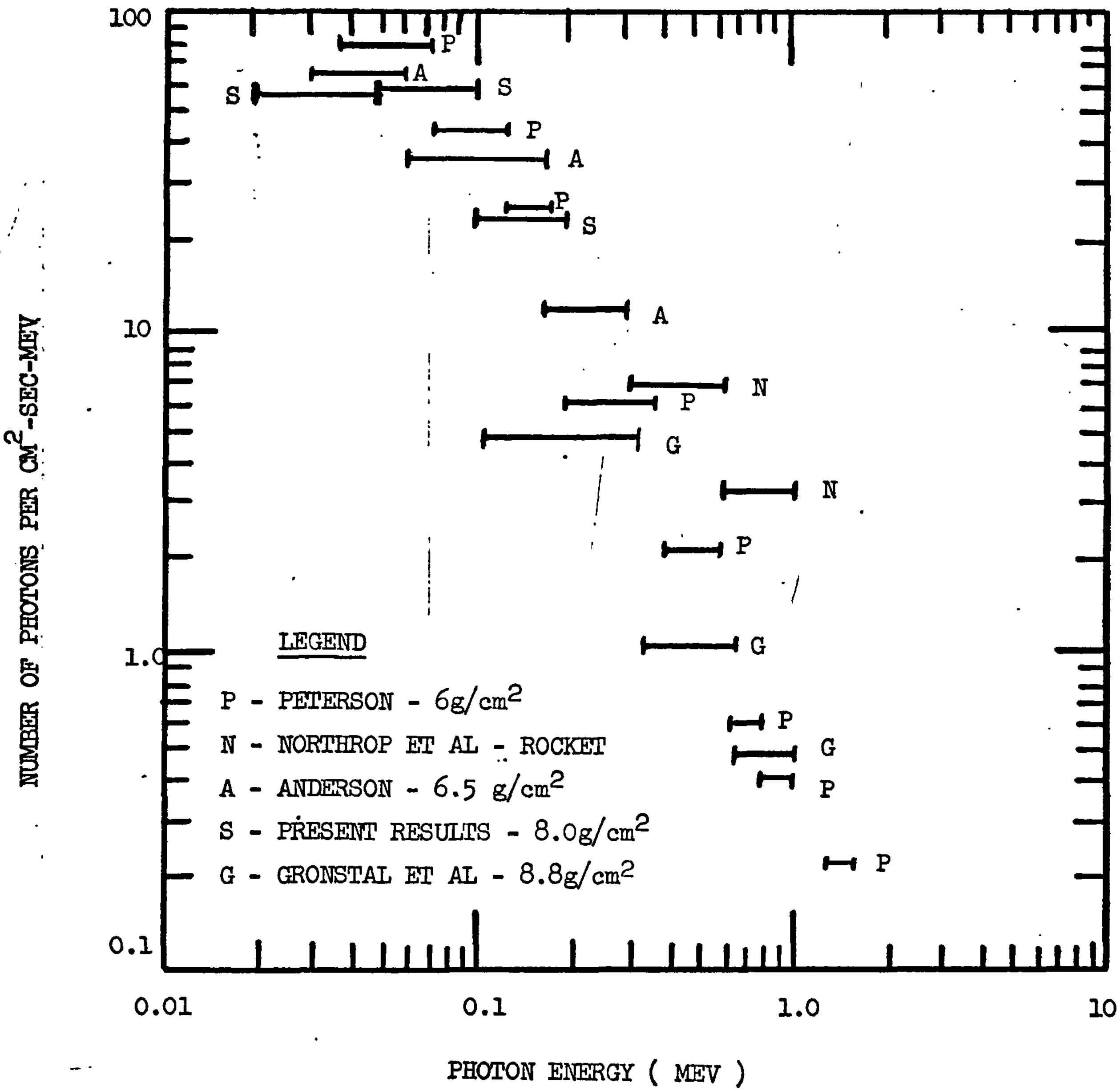
100
10
1.0
0.1
0.01
0.1
1.0
10
NUMBER OF PHOTONS PER CM2-SEC-MEV
PHOTON ENERGY (MEV)
LEGEND
P - PETERSON - 6g/cm2
N - NORTHROP ET AL - ROCKET
A - ANDERSON - 6.5 g/cm2
S - PRESENT RESULTS - 8.0g/cm2
G - GRONSTAL ET AL - 8.8g/cm2

Fig. 4

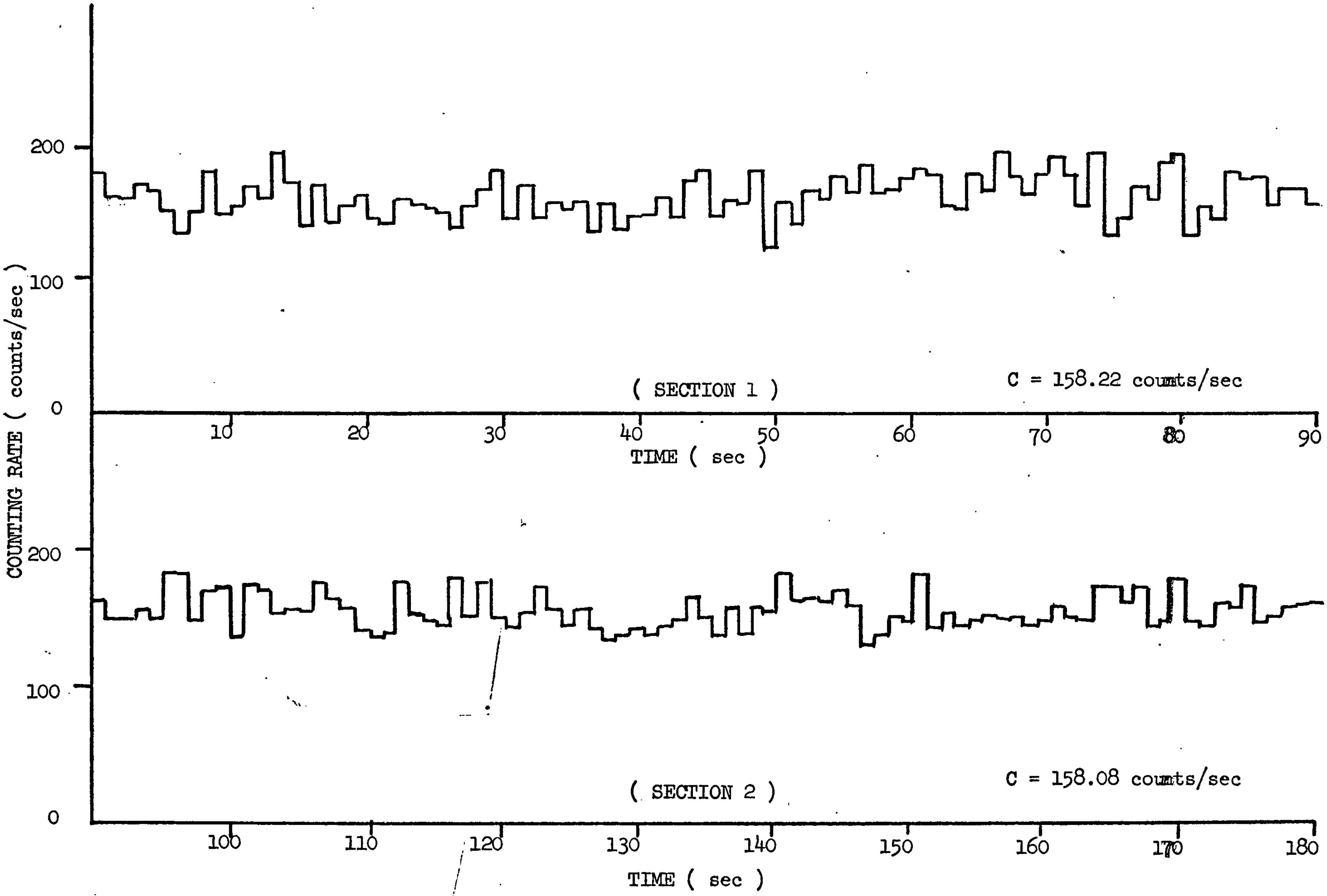
COUNTING RATE (counts/sec)
200
100
0
(SECTION 1)
C = 158.22 counts/sec
10
20
30
40
50
60
70
80
90
TIME (sec)
200
100
0
(SECTION 2)
C = 158.08 counts/sec
100
110
120
130
140
150
160
170
180
TIME (sec)

Fig. 5

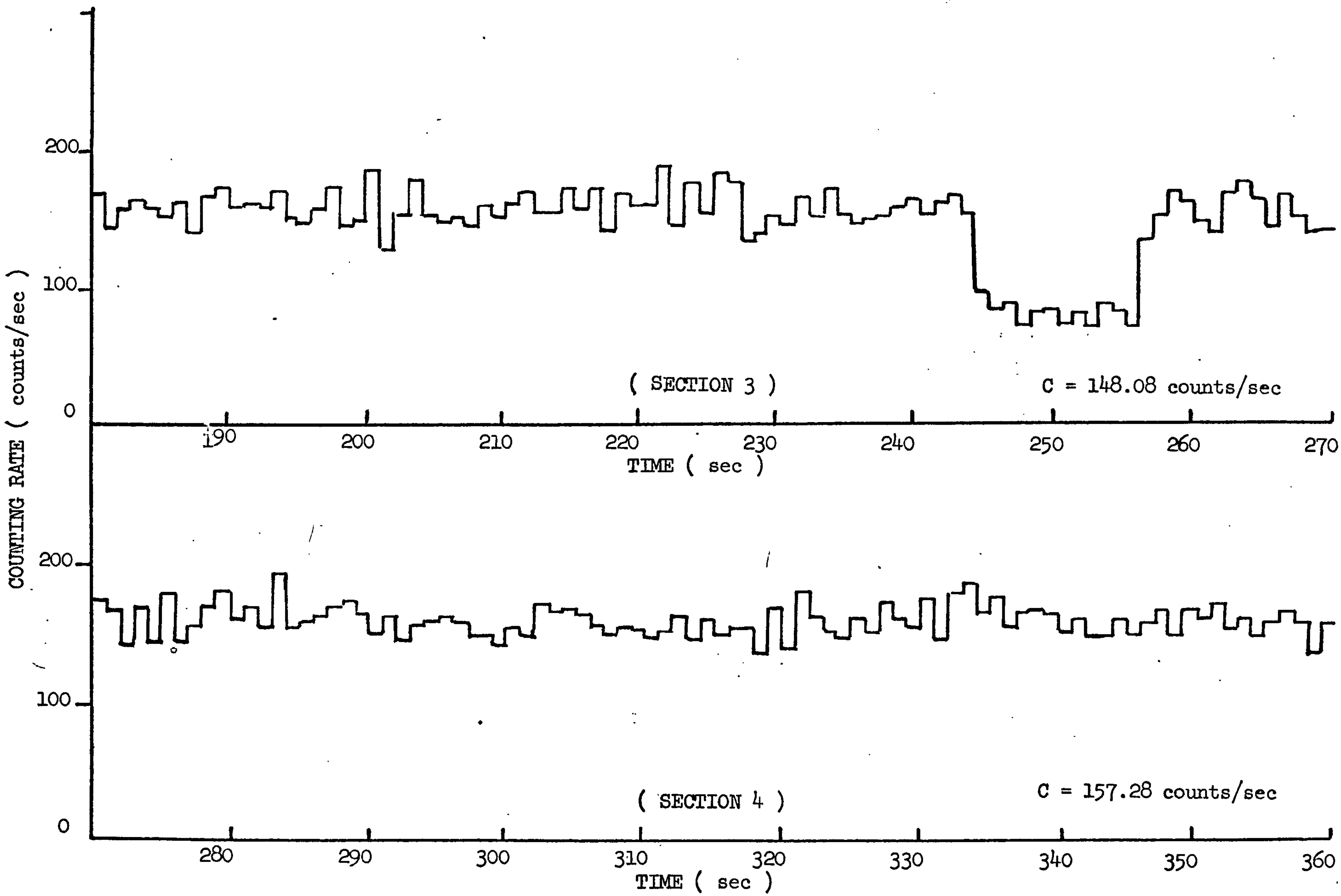
COUNTING RATE (counts/sec)
200
100
0
(SECTION 3)
C = 148.08 counts/sec
190
200
210
220
230
240
250
260
270
TIME (sec)
200
100
0
(SECTION 4)
C = 157.28 counts/sec
280
290
300
310
320
330
340
350
360
TIME (sec)

Fig. 5

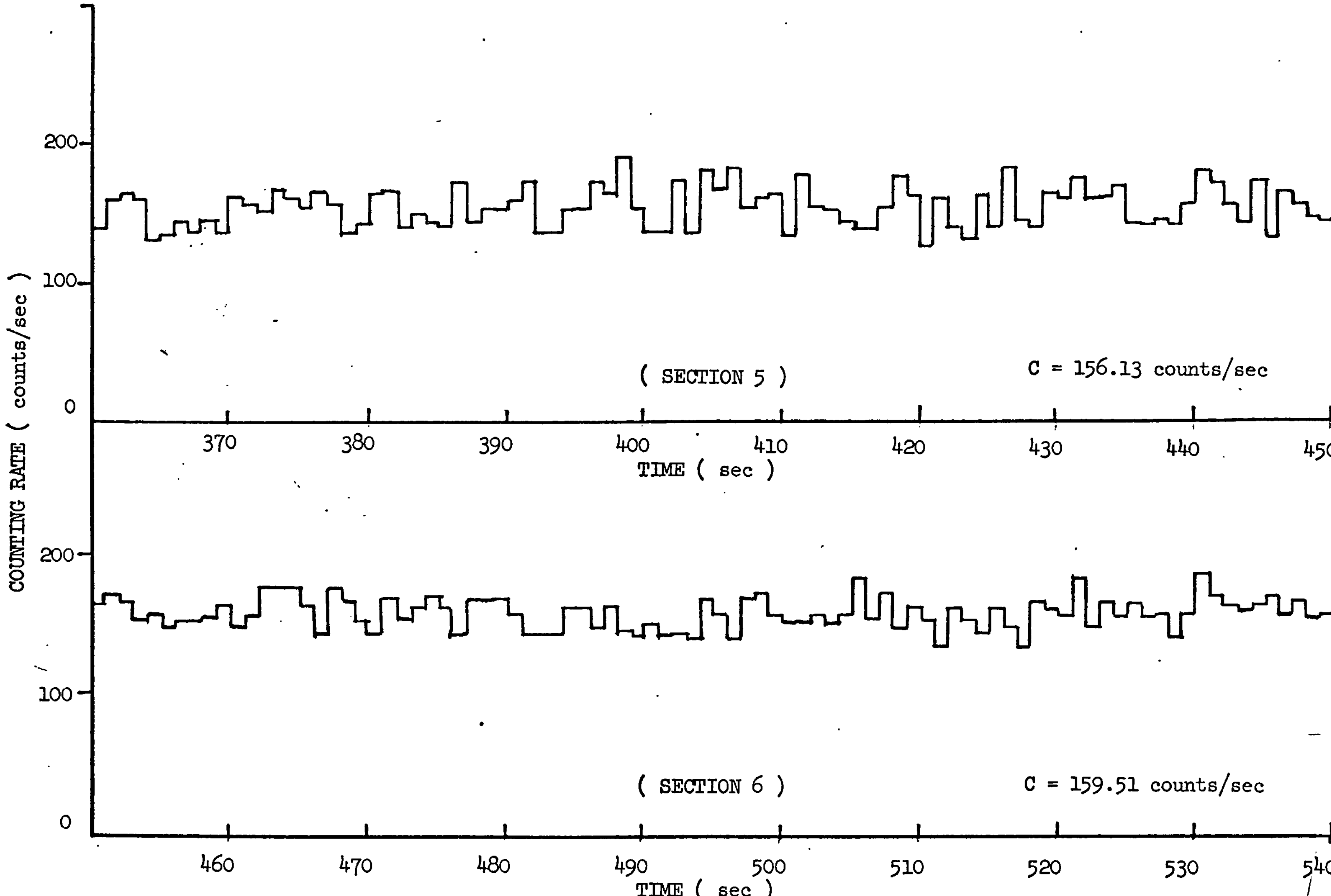
COUNTING RATE (counts/sec)
200
100
0
(SECTION 5)
C = 156.13 counts/sec
370
380
390
400
410
420
430
440
450
TIME (sec)
200
100
0
(SECTION 6)
C = 159.51 counts/sec
460
470
480
490
500
510
520
530
540
TIME (sec)

Fig. 5

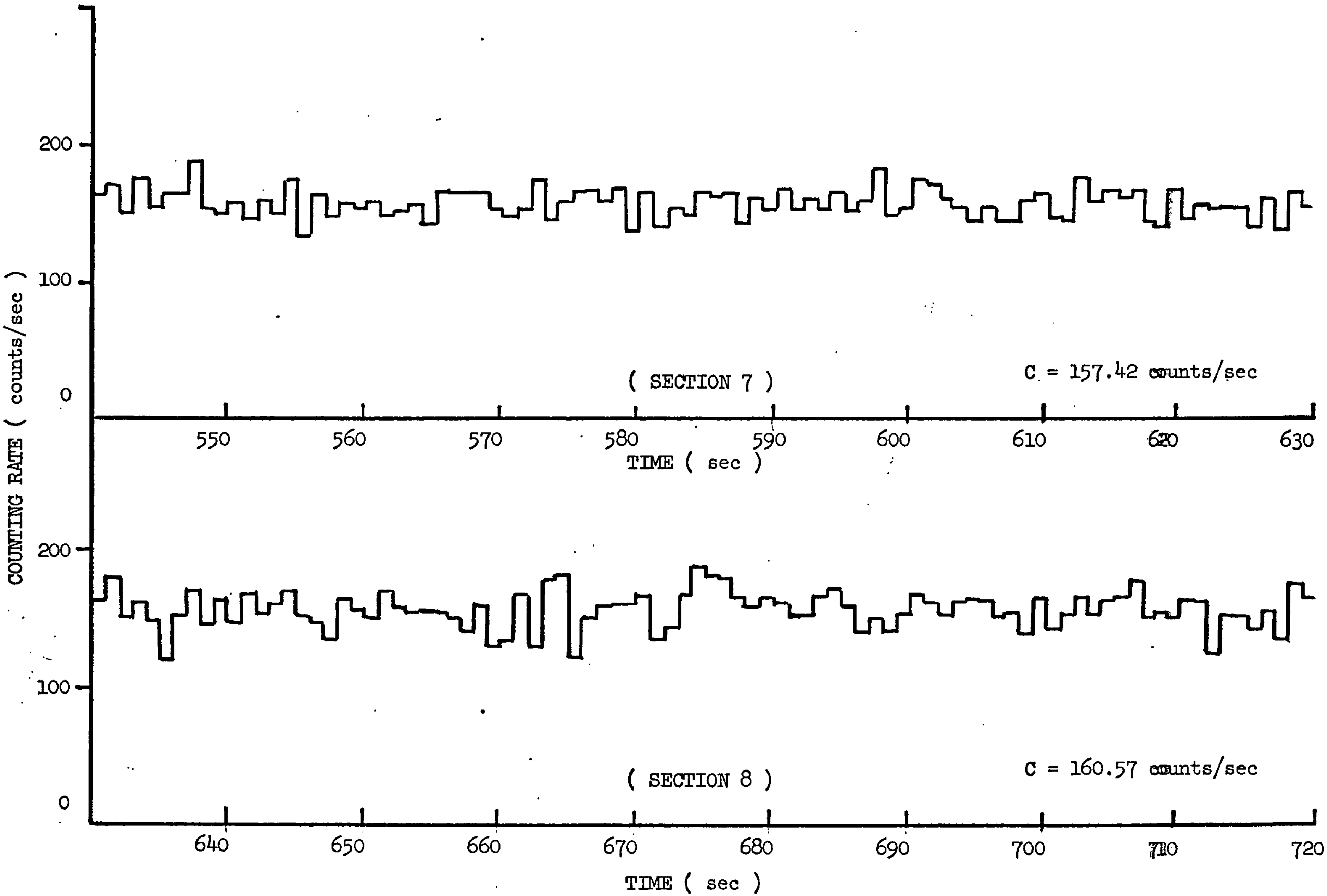

COUNTING RATE (counts/sec)
200
100
0
(SECTION 7)
C = 157.42 counts/sec
550
560
570
580
590
600
610
620
630
TIME (sec)
200
100
0
(SECTION 8)
C = 160.57 counts/sec
640
650
660
670
680
690
700
710
720
TIME (sec)

Fig. 5

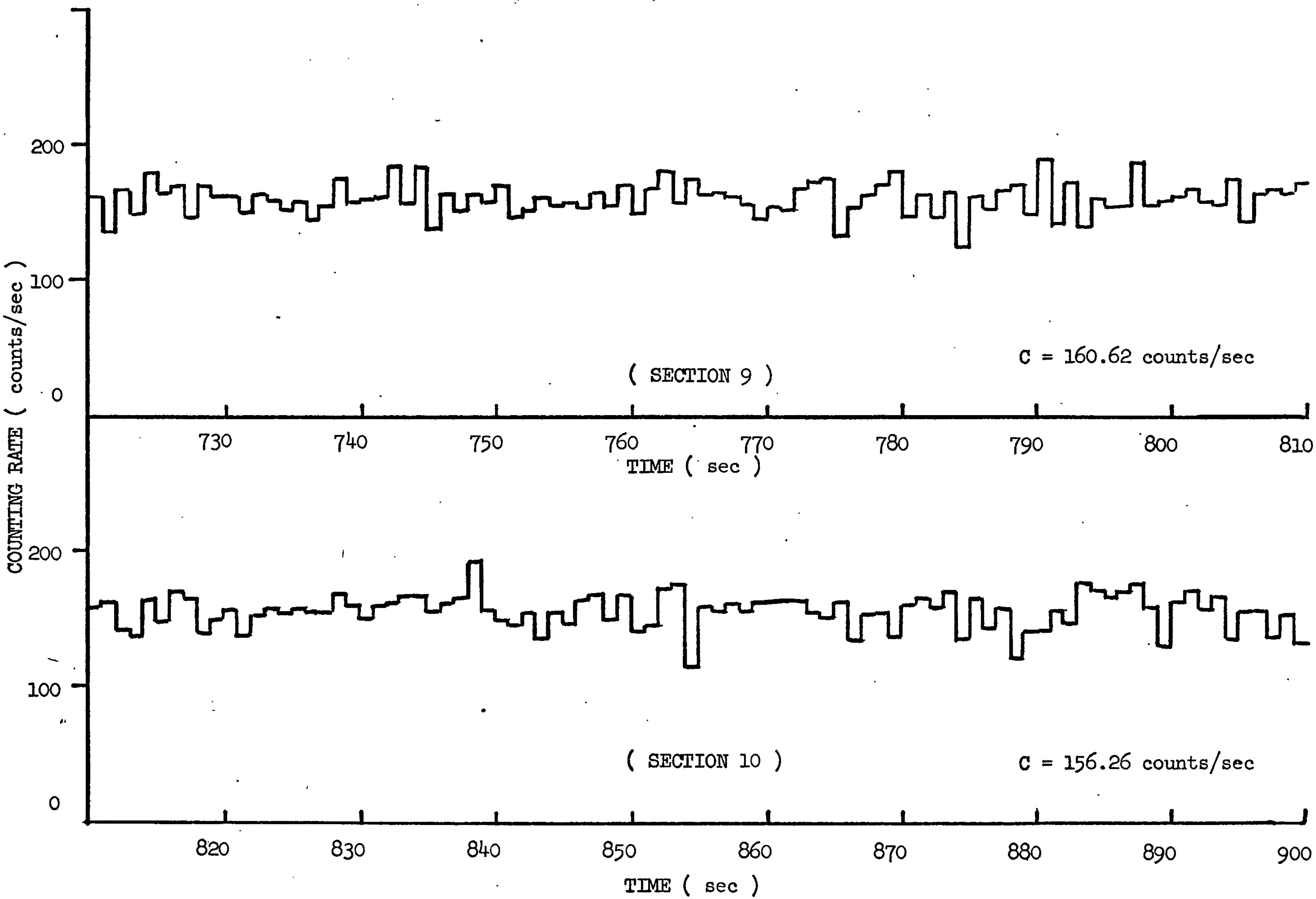

COUNTING RATE (counts/sec)
200
100
0
(SECTION 9)
C = 160.62 counts/sec
730
740
750
760
770
780
790
800
810
TIME (sec)
200
100
0
(SECTION 10)
C = 156.26 counts/sec
820
830
840
850
860
870
880
890
900
TIME (sec)

Fig. 5

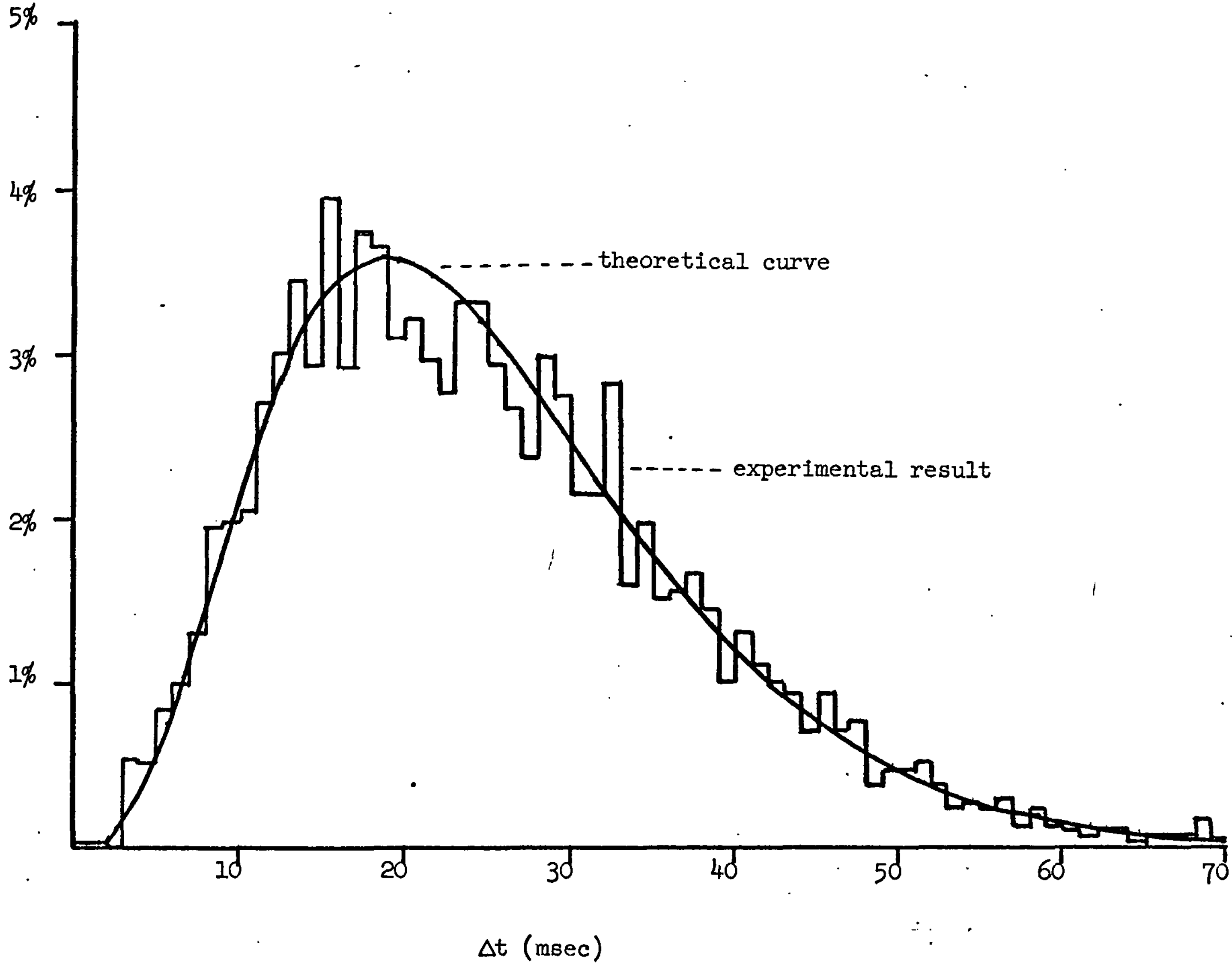
5%
4%
3%
2%
1%
theoretical curve
experimental result
10
20
30
40
50
60
70
Δt (msec)

Fig. 6

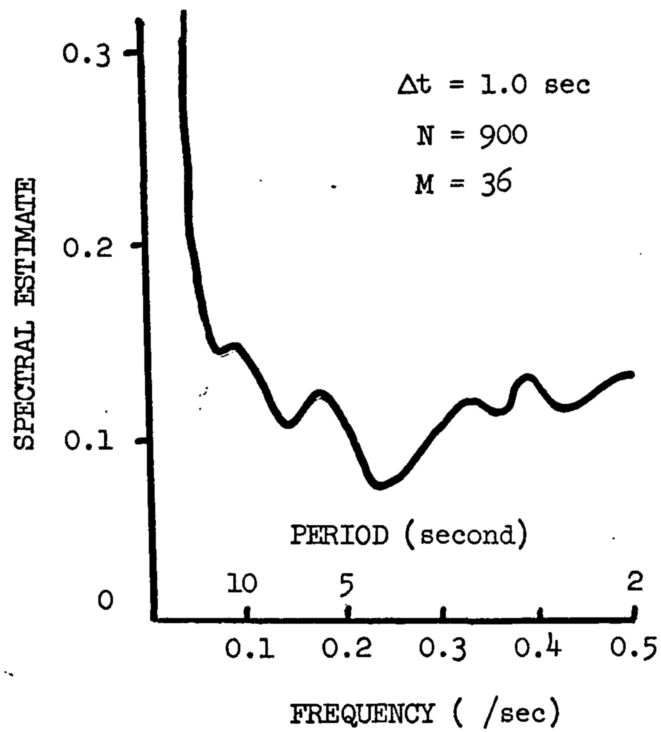

SPECTRAL ESTIMATE
0.3
0.2
0.1
0
Δt = 1.0 sec
N = 900
M = 36
PERIOD (second)
10
5
2
0.1
0.2
0.3
0.4
0.5
FREQUENCY (/sec)

Fig. 7

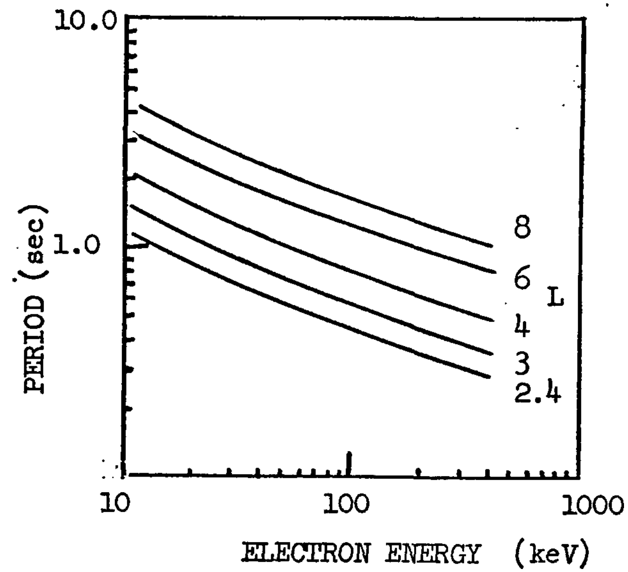

PERIOD (sec)
10.0
1.0
8
6
4
3
2.4
L
10
100
1000
ELECTRON ENERGY (keV)

Fig. 9

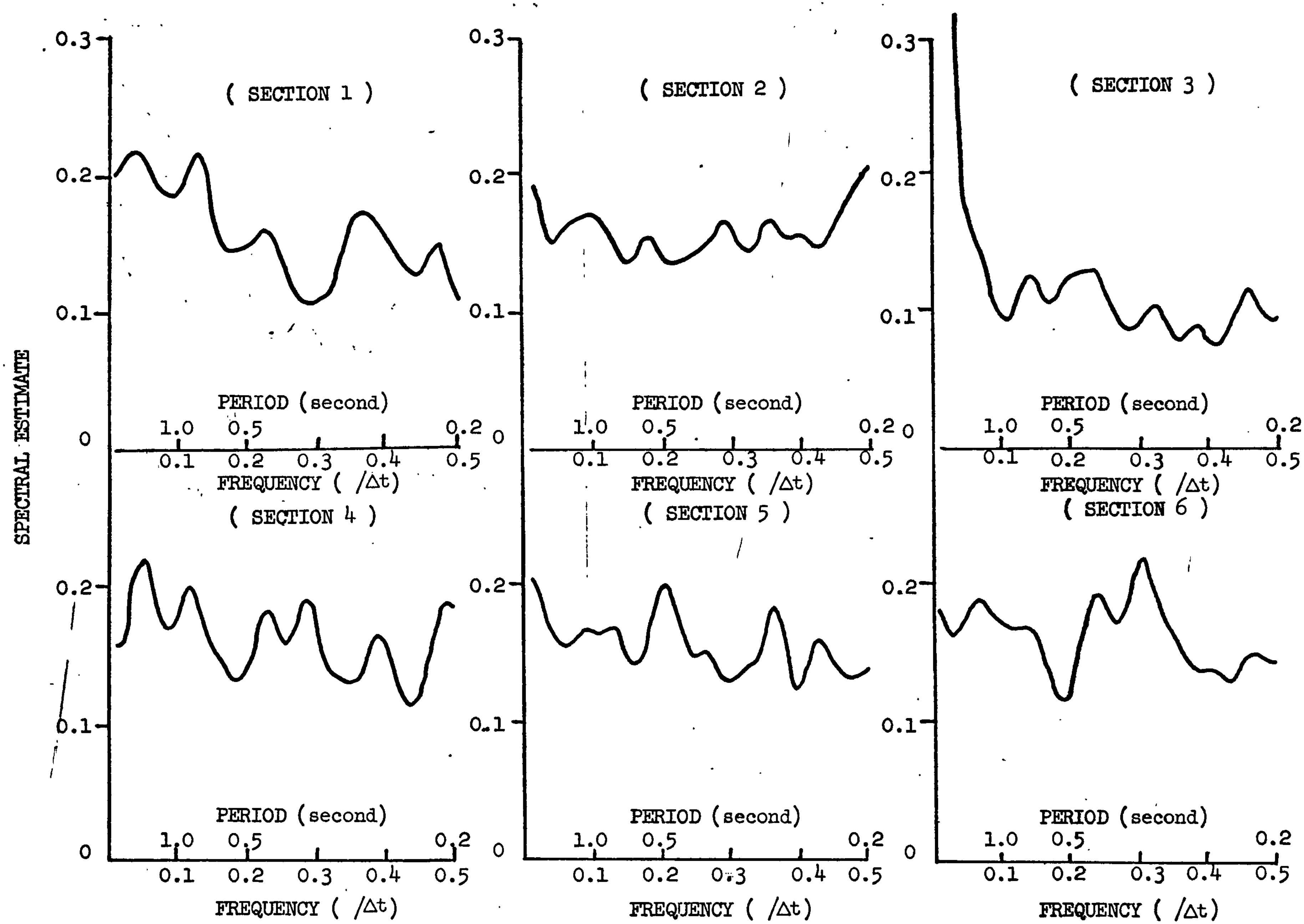
SPECTRAL ESTIMATE
(SECTION 1)
(SECTION 2)
(SECTION 3)
(SECTION 4)
(SECTION 5)
(SECTION 6)
0.3
0.2
0.1
0
PERIOD (second)
1.0 0.5 0.2
0.1 0.2 0.3 0.4 0.5
FREQUENCY (/Δt)

Fig. 8

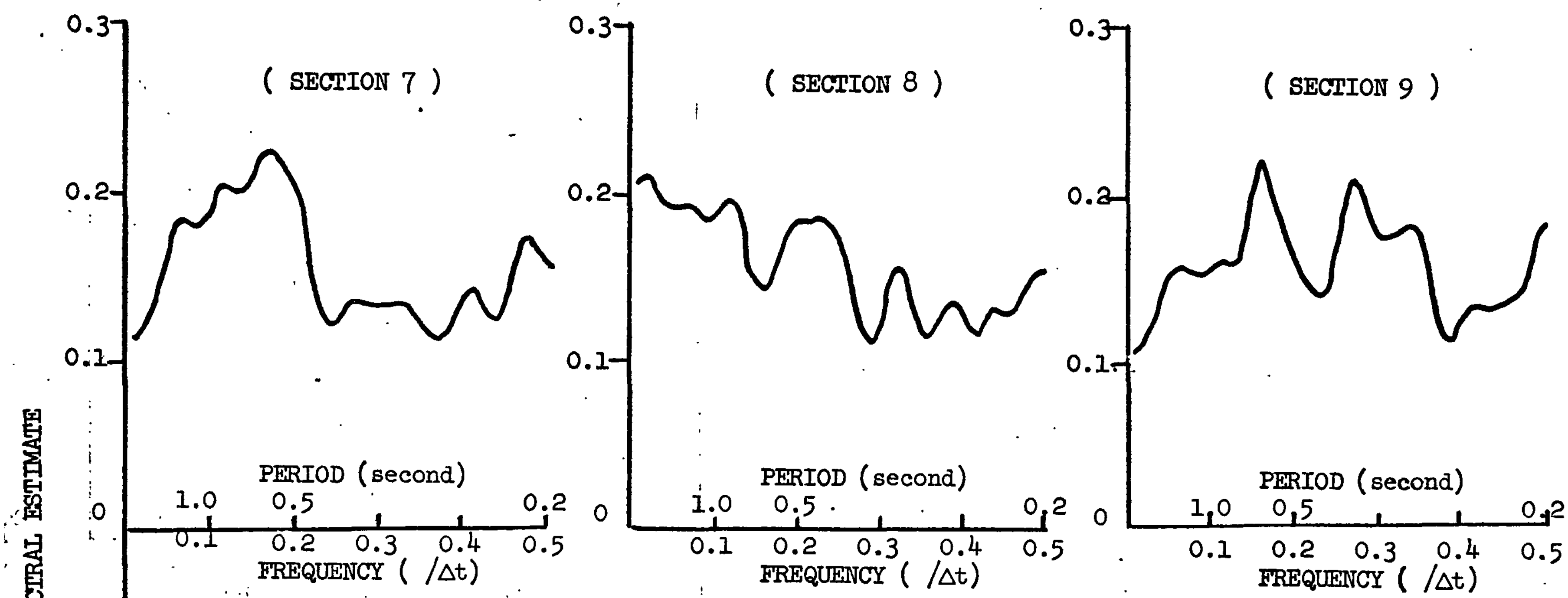

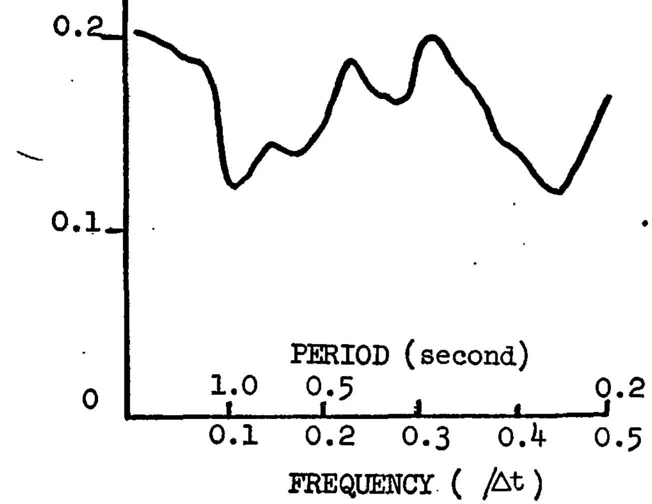

$\Delta t = 0.1$ sec

$N = 900$

$M = 36$

Fig. 8. Power Spectrum Computed For The Ten 90-sec Sections

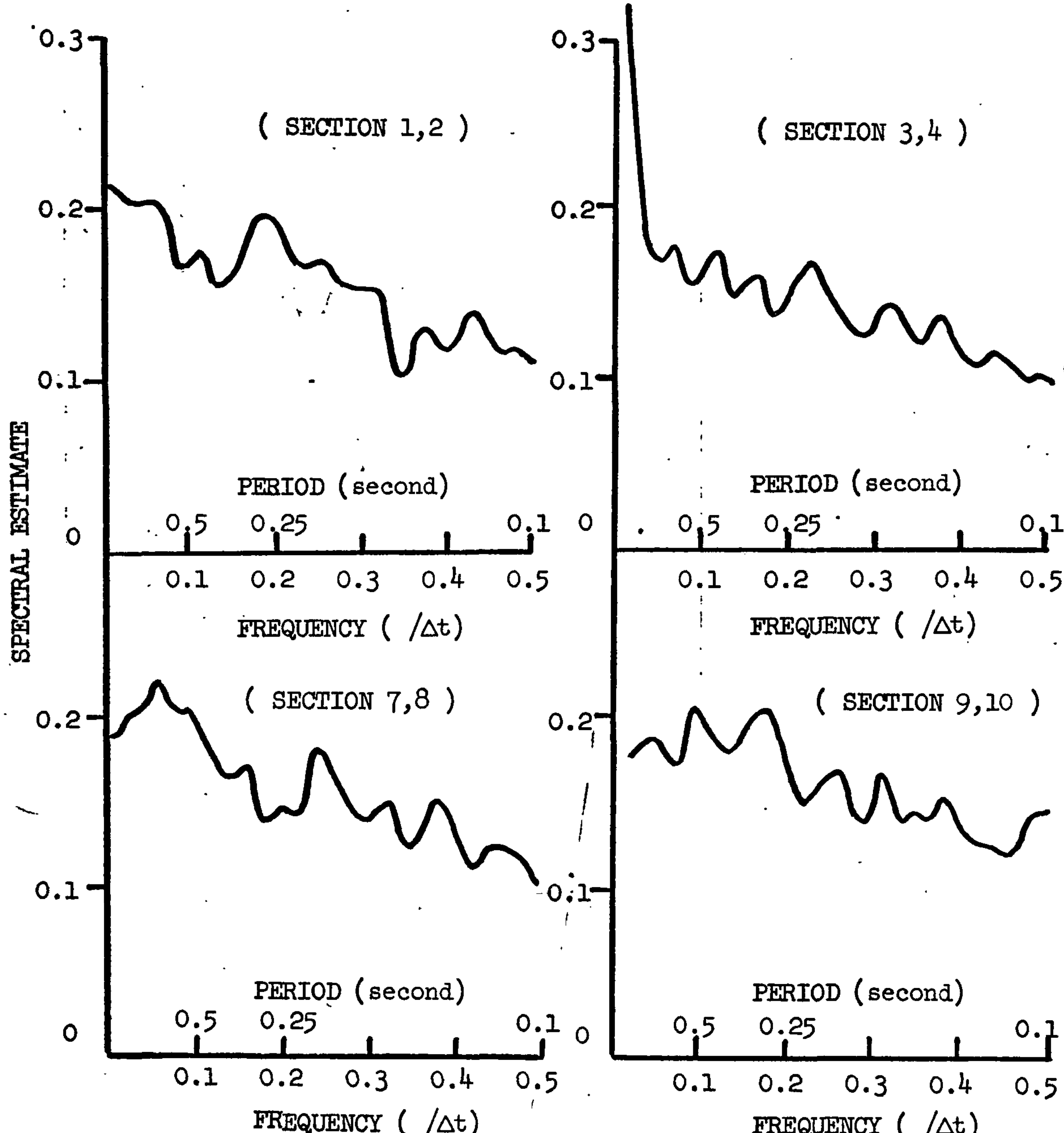

$\Delta t = 0.05$ sec

$N = 3600$

$M = 50$

Fig. 10 Power Spectral Computed For The Five 180-sec Sections

N	1	2	3	4	5	6	7	8	9	10
C	158.22	158.08	148.08	157.28	156.13	159.51	157.42	160.57	160.62	156.26
X^2	6.77	10.75	73.94	9.71	12.68	14.73	9.51	14.23	13.80	15.74

N = section number

C = average counting rate

X^2 = Chi-square

Table 1

REFERENCES

Anderson, K. A., A review of balloon measurements of X-rays in the auroral zone, University of California, Berkeley, 1964.

Anderson, K. A., and D. C. Enemark, Balloons of X-rays in the auroral zone II, J. Geophys. Res., 65, 3521-3538, 1960a.

Anderson, K. A;, C. D. Anger, R. R. Brown, and D. S. Evans, Simultaneous electron precipitation in the northern and southern auroral zones, J. Geophys. Res., 67, 4076-4077, 1962.

Anderson, K. A., and D. W. Milton, Balloon observations of X-rays in the auroral zone III, High time resolution studies, J. Geophys. Res., 69, 4457-4479, 1964.

Anger, C. D., J. R. Barcus, R. R. Brown, and D. S. Evans, Auroral zone X-ray pulsations in the 1- to 15-second range, J. Geophys. Res., 68, 1023-1030, 1963a.

Barcus, J. R., and A. Christensen, A 75 second periodicity in auroral zone X-rays, J. Geophys. Res., 70, 5455-5459, 1965.

Barcus, J. R., R. R. Brown, and T. J. Rosenberg, The spatial and temporal character of fast variations in the auroral zone X-ray, J. Geophys. Res., 71, 125-141, 1966.

Bhavsar, P. D., Scintillation counter observations of auroral X-rays during the geomagnetic storm of May 12, 1959, J. Geophys. Res., 66, 679-692, 1961.

Blake, J. B., S. C. Freden, and G. A. Paulikas, Precipitation of 400-keV electrons in the auroral zone, J. Geophys. Res., 5129-5134, 1966.

Blackman, R. B., and J. W. Tukey, The measurement of power spectra, Dover Publication, New York, 1959.

Brini, J. B., U. Ciriegi, F. Fuligni, and E. Moretti, Low-energy cosmic-ray photons in atmosphere, J. Geophys. Res., 72, 903-913, 1967.

Brown, R. R., Electron precipitation in the auroral zone, Space Science Reviews, 5, 311-382, 1966.

Evans, R. D., The atomic nucleus, McGraw-Hill, Inc., 1967.

Jenkins, G. M., General considerations in the analysis of spectra, Technometrics 3, 133-166, 1961.

Kern, J. W., Magnetosphere and Radiation Belts, Physics of geomagnetic phenomena, Vol. 2, Academic Press Inc., 1968.

Parzen, E., Notes on Fourier Analysis and Spectral Windows, Technical Report, No. 48, 1963.

Parzen, E., An approach to emirical time series analysis, Radio Science J. of Research, Vol. 68, No. 9, 1964.

O'Brien, B. J., Direct observations of dumping of electrons at 1000-km altitude and high latitudes, Vol. 67, No. 4, 1962. J. Geophys. Res.

O'Brien, B. J., High-latitude geophysical studies with satellite Injun 3.3. Precipitation of electrons into the atmosphere, J. Geophys. Res., 69, 13-43, 1964.

Oliven, M. N., Fast temporal variations in auroral zone X-rays, Master Thesis, University of Iowa, 1966.

Paulikas, G. A., and S. C. Freden, Precipitation of energetic electrons into the atmosphere, J. Geophys. Res., 69, 1239-1249, 1964.

Paulikas, G. A., J. B. Blake, and S. C. Freden, Precipitation of energetic electrons at middle latitudes, J. Geophys. Res., 71, 3165-3171, 1966.

Venkatesen, M. N., M. N. Oliven, P. J. Edwards, K. G. McCracken, and M. Steinbeck, Microburst Phenomena, 1. Auroral-zone X-rays, J. Geophys. Res. 73, 2333-2343, 1968.

Sonnett, C. P., and I. J. Abrams, The distant geomagnetic field, 3, J. Geophys. Res., 68, 1233-1263, 1963.

Winckler, J. R., P. D. Bhavsar, and K. A. Anderson, A study of the precipitation of energetic electrons from the geomagnetic field during magnetic storms, 67, 3717-3736, J. Geophys. Res., 1962.

Young, H. D., Statistical treatment of experimental data, McGraw-Hill, 1962.